Journal of Electromagnetic Waves and Applications

Publication details, including instructions for authors and subscription information:
http://www.tandfonline.com/loi/tewa20

Effect of nanostructured architecture on the enhanced optical absorption in silicon thin-film solar cells

Y.-C. Yao [a], M.-T. Tsai [b], P.-W. Lu [a], C.-J. Wu [a] & Y.-J. Lee [a]

[a] Institute of Electro-Optical Science and Technology, National Taiwan Normal University, Taipei, 116, Taiwan, ROC

[b] Department of Electrical Engineering, Chang Gung University, Tao-Yuan, 333, Taiwan, ROC

Version of record first published: 01 Aug 2012.

To cite this article: Y.-C. Yao, M.-T. Tsai, P.-W. Lu, C.-J. Wu & Y.-J. Lee (2012): Effect of nanostructured architecture on the enhanced optical absorption in silicon thin-film solar cells, Journal of Electromagnetic Waves and Applications, 26:13, 1798-1807

To link to this article: http://dx.doi.org/10.1080/09205071.2012.713189

Journal of Electromagnetic Waves and Applications
Vol. 26, No. 13, September 2012, 1798–1807

Taylor & Francis
Taylor & Francis Group

Effect of nanostructured architecture on the enhanced optical absorption in silicon thin-film solar cells

Y.-C. Yao[a], M.-T. Tsai[b], P.-W. Lu[a], C.-J. Wu[a] and Y.-J. Lee[a]*

[a]*Institute of Electro-Optical Science and Technology, National Taiwan Normal University, Taipei 116, Taiwan, ROC;* [b]*Department of Electrical Engineering, Chang Gung University, Tao-Yuan 333, Taiwan, ROC*

(*Received 27 May 2012; accepted 11 July 2012*)

We apply the finite-difference time-domain method to numerically calculate the enhanced optical absorption of three nanostructures (i.e. nanorod, nanocone, and nanolens arrays) that were decorated on the surface of 2 μm thick crystal silicon (Si) thin-films. Compared with the nanorod and nanocone arrays, the nanolens array exhibits the highest power conversion efficiency. This result is mainly attributed to the natural capability of the nanolens array to optically couple incident light into in-plane guided modes, which increases the optical path of the incident photons in the long-wavelength regime. The power conversion efficiencies of the optimized nanorod, nanocone, and nanolens arrays are $\eta = 17.4$, 18.8, and 22.0%, respectively. These efficiencies correspond to enhancements of 26.1, 36.2, and 59.4% for the nanorod, nanocone, and nanolens arrays, respectively, compared with a planar Si thin-film with a standard quarter-wavelength antireflection layer. These findings show promises for the nanostructured design of Si thin-film solar cells that exhibit enhanced optical absorption.

1. Introduction

Developing solar cells with high conversion efficiency has become increasingly important as the demand for solar energy has increased [1,2]. Silicon (Si) is widely used in photovoltaic applications because of its abundant supply and mature fabrication process [3].

Through the use of nanostructures, the reflectance from the surface of Si solar cell has been reduced, which is beneficial for harvesting incident sunlight [4–8]. Various nanostructured arrays (e.g. randomly or periodically aligned nanorods (or nanowires) [9–14], nanocones [15–17], and nanodomes [18–21]) have been proposed to improve the conversion efficiency of solar cells. For example, recently Zhu et al. [15] demonstrated that the optical absorption of hydrogenated amorphous silicon (a-Si:H) in $\lambda = 400$–800 nm is significantly enhanced of nanowires (70%) and nanocones (88%) arrays, comparing to the planar thin-film structure (53%). Additionally, the optical absorption of a-Si:H can be further enhanced to 94% while adopting the nanodome arrays [20]. Theoretical and experimental studies have indicated that nanostructured arrays can suppress optical reflections and promote the trapping of incident photons [22]. These properties alleviate the requirements for Si quality and increase the feasibility of Si thin-film solar cells. Although Si nanostructures have been extensively studied,

*Corresponding author. Email: yajulee@ntnu.edu.tw

ISSN 0920-5071 print/ISSN 1569-3937 online

http://dx.doi.org/10.1080/09205071.2012.713189
http://www.tandfonline.com

the effect of nanostructured architectures on enhanced optical absorption and optimized photovoltaic efficiency of photovoltaic devices has rarely been reported, and this information is important for guiding the development of advanced photovoltaic devices. In this study, we use the finite-difference time-domain (FDTD) method to investigate the dependence of various nanostructured arrays (including nanorods, nanocones, and nanolenses) on the enhanced optical absorption and power conversion efficiency of Si thin-film solar cells [23,24]. The diameter and periodicity of nanostructured arrays considerably affect the corresponding optical absorption spectrum. By appropriately arranging the periodicity of the nanostructured array, the incident light that penetrates the crystal Si can be coupled into in-plane guided modes, increasing the optical path of the emitting photons and the power conversion efficiency of the solar cell. As a result, an power conversion efficiency of $\eta = 17.4$, 18.8, and 22.0% can be obtained for 2 μm-thick Si films decorated with the optimized dimensions of the nanorod, nanocone, and nanolens arrays, respectively.

2. Structure model and analysis method

Figure 1(a) shows a schematic of the nanostructures studied here, including (left) the nanorod, (center) nanocone, and (right) nanolens arrays, decorated on a crystal Si with a total thickness of 2 μm. These nanostructured arrays are arranged in a square lattice with a periodicity of P in the x and y directions and a depth H in the z direction. The effective refractive index (n_{eff}) of the nanostructured arrays is defined as the refractive index between the air and the bare Si, weighted by their respective volumes and governed by the Bruggeman model as follows [25]:

$$f_{\text{Si}}(z) \cdot \frac{n_{\text{Si}}^2 - n_{\text{eff}}^2}{n_{\text{Si}}^2 + 2n_{\text{eff}}^2} + f_{\text{air}}(z) \cdot \frac{n_{\text{air}}^2 - n_{\text{eff}}^2}{n_{\text{air}}^2 + 2n_{\text{eff}}^2} = 0, \tag{1}$$

where n_{Si} and n_{air} refer to the refractive indices of crystalline Si and air, respectively; $f_{\text{Si}}(z)$ and $f_{\text{air}}(z)$ are the weighting coefficients and $f_{\text{Si}}(z) + f_{\text{air}}(z) = 1$. $f_{\text{Si}}(z)$ can be expressed as

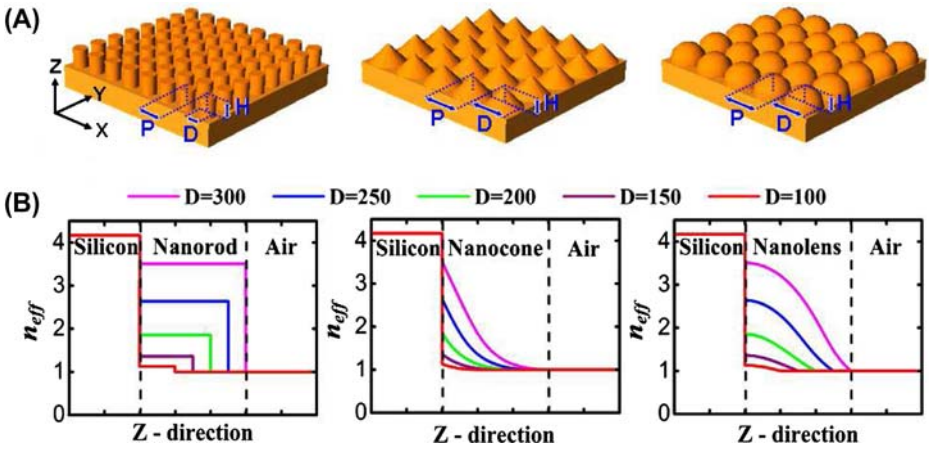

Figure 1. (A) A schematic of the nanostructured arrays, including the (left) nanorod, (center) nanocone, and (right) nanolens arrays for the computational simulations. (B) The corresponding effective refractive index profiles along the z direction with increasing $D(z)$.

$f_{Si}(z) = \frac{\pi}{P^2}(\frac{D(z)}{2})^2$, where D($z$) is the diameter of the nanostructured arrays, which varies along the z direction ($0 \leq z \leq H$), and is defined for the different arrays as follows:

$$D(z) = 2H, \quad \text{for nanorod} \tag{2}$$

$$D(z) = 2(H - z), \quad \text{for nanocone} \tag{3}$$

$$D(z) = 2\sqrt{H^2 - z^2}, \quad \text{for nanolens} \tag{4}$$

Figure 1(b) shows the corresponding profiles of the effective refractive indices along the z direction for all of the nanostructured arrays as D ($z = 0$) increases from 100 to 300 nm with a 50 nm interval and a fixed $P = 300$ nm [see the discussion in Figure 3(a)]. The FDTD method is employed to simulate the interaction between the incident light and the nanostructured arrays depicted in Figure 1(a) by adopting periodic boundary conditions in the x and y directions and a perfectly matched layer boundary condition in the z direction. The propagation of the incident light is set to $\vec{k} = k_z\hat{k}$ with the electric field oscillating in the x direction (*TE* polarization, $\vec{E} = E_x\hat{i}$). The electromagnetic field distribution of the light waves at a certain position of nanostructured arrays was obtained by solving the time-harmonic Maxwell's equations as follows:

$$\nabla \times \nabla \times \vec{E}(\vec{r}) - n^2 k_0^2 \vec{E}(\vec{r}) = 0, \tag{5}$$

$$\nabla \times \left(\frac{1}{n^2}\nabla \times \vec{H}(\vec{r})\right) - k_0^2 \vec{H}(\vec{r}) = 0, \tag{6}$$

where n is the complex refractive index and k_0 the magnitude of the free-space wave vector. Consequently, the spatial distributions of the energy flux, i.e. the reflectance (R), transmittance (T), and absorption (A), can therefore be determined by:

$$R = |r_s|^2 = \left|\frac{\eta_2 \cos\theta_i - \eta_1 \cos\theta_t}{\eta_2 \cos\theta_i + \eta_1 \cos\theta_t}\right|^2, \tag{7}$$

$$T = |t_s|^2 = \left|\frac{2\eta_2 \cos\theta_i}{\eta_2 \cos\theta_i + \eta_1 \cos\theta_t}\right|^2, \tag{8}$$

$$A = 1 - R - T, \tag{9}$$

where r_s and t_s are reflection and transmission coefficients of *TE* polarized light, respectively. $\eta_{1,2} = \sqrt{\mu_{1,2}/\varepsilon_{1,2}}$ represent the intrinsic impedance in the different mediums. θ_i and θ_t are the angles of incidence and transmission, respectively.

To evaluate the performances of the nanostructured arrays, the current density (J) vs. the voltage (V) is expressed as the sum of the photon-generated current minus the intrinsic current generated by radiative recombination as follows [26]:

$$J(V) = \frac{q}{hc}\int_0^\infty \lambda \frac{dI}{d\lambda} A(\lambda) d\lambda - \frac{q(n^2+1)E_g^2 kT}{4\pi\hbar^3 c^2} e\left(\frac{eV - E_g}{kT}\right), \quad (10)$$

where $dI/d\lambda$ represents the light intensity incident on the solar cell per unit wavelength, $A(\lambda)$ is the corresponding absorption spectrum, E_g is the band gap energy of Si, kT is the thermal energy, and n is the refractive index of Si.

The power conversion efficiency (η) for all of the nanostructured arrays by using the formula [27]:

$$\eta = \frac{J_{SC} \cdot V_{OC} \cdot FF}{\int_0^\infty I(\lambda) d\lambda}, \quad (11)$$

where $I(\lambda)$ represents the solar energy density spectrum as depicted in Figure 2(a), J_{SC} is the short-circuit current density (found by substituting $V = 0$ in Equation (5)), V_{OC} is the open-circuit voltage, and FF is the fill factor.

3. Numerical results and discussion

Figure 2(a) shows a typical solar spectrum [28]. In this work, we mainly investigated incident light with an emitting wavelength of $\lambda = 320$–1000 nm, including the primary part of solar energy (marked by blue dashed line). Figure 2(b) plots the absorption spectra of the three representative nanostructured arrays described in Figure 1(a) with different diameters [$D(z=0) = 100$, 200, 250, and 300 nm] and a fixed $P = 300$ nm. The absorption spectrum of a planar Si thin-film (black solid line) is also plotted in the figure for comparison.

The calculated J–V curves of the nanostructured arrays using Eq. (10) are shown in the insert of Figure 2(b). By fixing $P = 300$ nm, the optical absorption of nanorod arrays increases initially with $D(z)$ up to 200 nm and then decreases with further increases in $D(z)$ to 250–300 nm, leading to the maximum J_{SC} of the nanorod arrays with $D(z)$ = 200 nm [J_{SC} for $D(z) = 200$ nm $> D(z) = 300$ nm $> D(z) = 100$ nm]. It is because its ($D(z) = 200$ nm) effective refractive index is approximately equal to the geometric mean of those of the air and bare Si [see Figure 1(b)] that the destructive interference with extremely low reflection is supported for incident light in the short-wavelength regime ($\lambda < 600$ nm). This observation agrees with previous reports [9,11,13]. However, for the nanocone and nanolens arrays, the corresponding optical absorption spectra increase monotonically, leading to a increasing of J_{SC} with $D(z)$ [J_{SC} for $D(z) = 300$ nm $> D(z) = 200$ nm $> D(z)$ = 100 nm]. It is primarily due to the much continuous profiles of the refractive index along the z direction with increasing $D(z)$, providing excellent impedance matching between the Si and air. Clearly, as shown in Figure 1(b), the discontinuity of refractive index along the z direction is less significant with increasing $D(z)$ for both nanocone and nanolens arrays. Consequently, incoming photons from the air confront much gradual change of the refractive index with increasing $D(z)$, which creates a broadband antireflection (AR) layer and thus eliminates the reflection of solar energy [29–31]. Hence, the ratio of $D(z=0)/P$ for the nanocone and nanolens arrays is set to $D(z=0)/P = 300/300$ nm here. Generally, the J–V curves for all of the nanostructured arrays shown in Figure 2 (b) have a similar trend as the optical absorption spectra, which agree with Equation (10).

Figure 2(c) shows the optical absorption spectra for all of the nanostructured arrays arranged in different periodicities ($P = 100$, 300, and 500 nm). The corresponding J–V curves are also shown in the figure. The optical absorption spectra strongly depend on the periodicities of the nanostructured arrays. For $P = 100$ nm, all of the nanostructured arrays exhibit

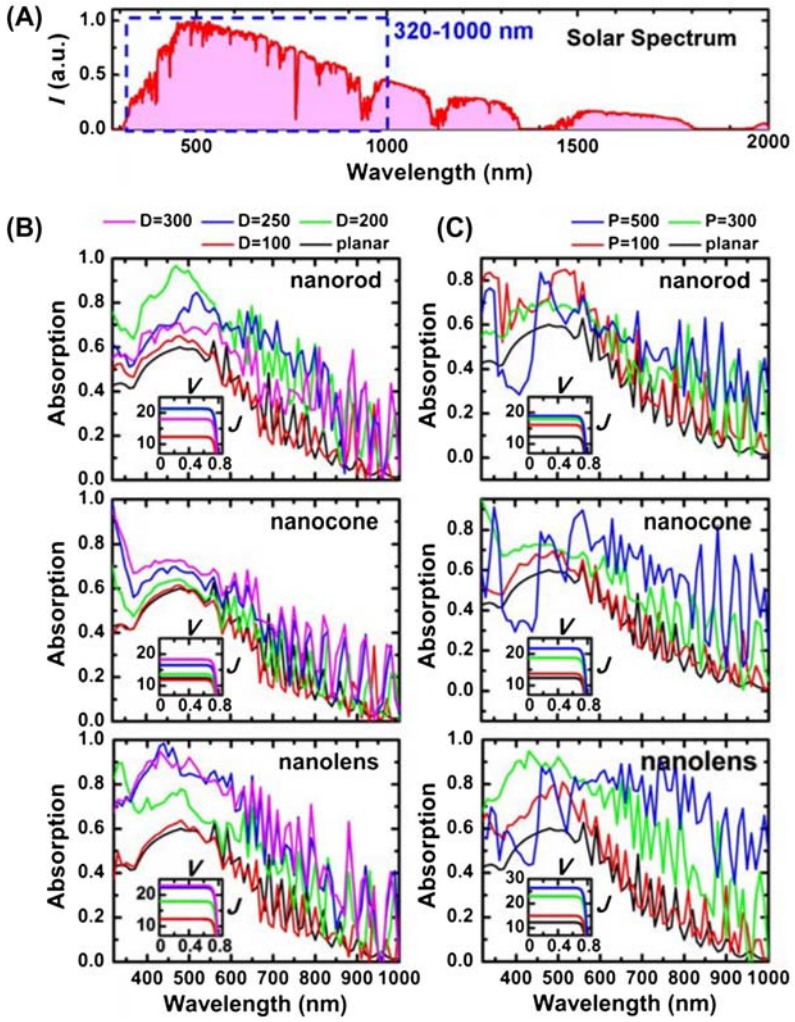

Figure 2. (A) ASTM air mass 1.5 direct and circumsolar solar spectrum. (B) The optical absorption spectra of the nanostructured arrays for different array diameters: $D(z=0)=100$, 200, 250, and 300 nm. The array periodicity is set to $P=300$ nm. (C) The optical absorption spectra of all of the nanostructured arrays arranged in different periodicities ($P=100$, 300, and 500 nm). Inset: the corresponding J–V curves calculated by Equation (5) for the nanostructured arrays with different diameters and periodicities.

optical absorption spectra that are similar to a planar Si thin-film in the long-wavelength regime, and the absorption is only enhanced at wavelengths shorter than $\lambda=600$ nm. When P is increased to $P=300$ nm, the optical absorption spectra for all of the nanostructured arrays are considerably enhanced across the entire range of incident wavelengths, especially for the nanolens array. When P is further increased to $P=500$ nm, the optical absorptions of the nanostructured arrays are mainly enhanced in the long-wavelength regime ($\lambda>600$ nm), and they become lower than the absorption of a planar Si thin-film in the short-wavelength regime ($350\text{ nm}<\lambda<450$ nm). This behavior can be explained by fundamental physical optics. For short periodicities, incident light with long wavelengths will not interact with the nanostructured arrays, and it will penetrate the array, leading to a similar optical spectrum as a planar Si thin-film. When the periodicity of the nanostructured array is near the incident light

wavelength, then strong diffraction and optical coupling of the incoming photons are expected, prolonging the optical path of the incoming photons within the solar cells and enhancing the total optical absorption. Thus, for $P = 100$ nm, the optical absorption is primarily enhanced in the short-wavelength regime. It is also reasonable that the optical absorption is shifted to the long wavelength regime as P of nanostructured arrays increases, and will be even worse than the one of planar Si thin-film in the short wavelength regime. Most importantly, this shift indicates that the periodicity of nanostructured arrays can considerably affect the enhanced optical absorption of incident light and must be appropriately optimized for the individual shapes of the nanostructured arrays.

Figure 3 plots the power conversion efficiency (η) vs. (a) diameter and (b) periodicity for all of the nanostructured arrays by using Eq. (6). J_{SC} as a function of D and P for the nanostructured arrays are also shown in the figure. The power conversion efficiencies of the planar Si thin-film with ($\eta = 13.8\%$) and without ($\eta = 9.8\%$) the quarter-wavelength AR layer are marked in the figure to serve as references. By fixing $P = 300$ nm [Figure 3(a)], the maximum efficiencies ($\eta = 17.0$, 14.9, and 18.7%) are obtained for the nanorod [$D(z = 0) = 250$ nm], nanocone [$D(z = 0) = 300$ nm], and nanolens [$D(z = 0) = 300$ nm] arrays, respectively. While appropriately arranging the periodicity of the nanostructured arrays (Figure 3(b)), optimized efficiencies of $\eta = 17.4$, 18.8, and 22.0% can be obtained for the nanorod ($P = 400$ nm), nanocone ($P = 500$ nm), and nanolens ($P = 500$ nm) arrays, respectively, and these efficiencies correspond to enhancements of approximately 26.1, 36.2, and 59.4%, respectively, when compared with the planar Si thin-film with an AR layer.

To elucidate the physical mechanisms involved in the enhanced efficiency of nanostructured arrays, Figure 4 shows the distribution of the simulated electric field for (a) $\vec{E}_x$ and (b) $\vec{E}_z$ in the nanostructured arrays for incident wavelengths of $\lambda = 400$, 600, and 800 nm. At $\lambda = 400$ nm, the extinction coefficient (κ) of crystal Si is relatively large; therefore, the incident light is almost absorbed immediately in a single path near the top of all of the nanostructured arrays. Thus, the coupling or diffraction of incident light with the nanostructured arrays is irrelevant in the short-wavelength regime. In contrast, the incident light penetrating the nanostructured arrays becomes more problematic with increasing incident wavelength because κ decreases rapidly [32]. Thus, the crystal Si is less absorptive in the long-wavelength regime. This result indicates that prolonging the optical path of

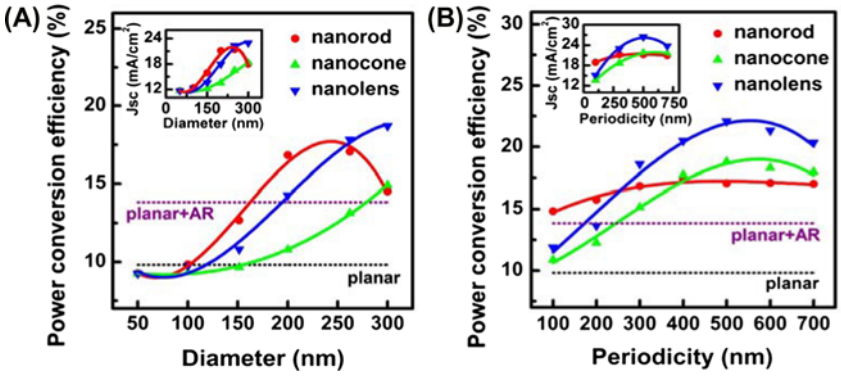

Figure 3. The power conversion efficiency vs. (A) the diameter and (B) the periodicity of the nanostructured arrays. Planar Si thin-film solar cells with ($\eta = 13.8\%$) and without ($\eta = 9.8\%$) the AR layer serve as references. Insert: the short-circuit current density vs. diameter and periodicity of the nanostructured arrays.

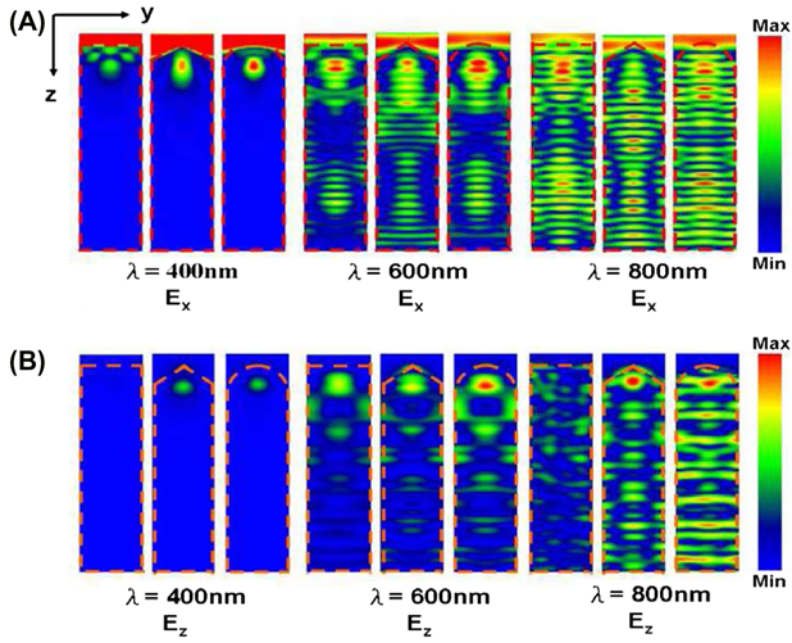

Figure 4. The distributions of the simulated electric field of (A) E_x and (B) E_z in the nanostructured arrays for the incident wavelengths ($\lambda = 400$), 600, and 800 nm.

incoming photons in crystal Si is necessary for long incident wavelengths. As shown in Figure 4(b), the nanostructured arrays, particularly the nanolens array because it has the strongest integrated intensity of $\vec{E}_z$, can couple the incident light into optical modes ($\vec{k} = k_x\hat{i} + k_y\hat{j}$) guided within the crystal Si. This finding is consistent with the results shown in Figures 2 and 3, in which the nanolens array exhibits higher optical absorption and superior power conversion efficiency compared with the other nanostructures.

To study the dependence of the optical absorption of nanostructured arrays on the incident angle of solar illumination, Figure 5 shows the optical absorption $A(\theta, \lambda)$ as a function of the incident wavelength (λ) and the oblique angle (θ) for the optimized nanostructured arrays [33,34]. $A(\theta, \lambda)$ of the planar Si thin-film is also calculated and shown in Figure 5(a) for comparison. For the incident wavelengths studied here, $A(\theta, \lambda)$ decreased with increasing oblique angle because of the enhancement of reflectivity governed by the Fresnel equation for the incidence of *TE* polarized light [35]. The nanolens array shows the highest optical absorption, particularly for incident wavelength ranging from $\lambda = 350$–600 nm. This wavelength range covers the highest energies from solar illumination (Figure 2(a)). Similarly, Figure 6 presents the power conversion efficiency (η) as a function of the array periodicity and oblique angle for the (a) nanorod, (b) nanocone, and (c) nanolens arrays. An optimal range of parameter space exists that maximizes the power conversion efficiency for all of the nanostructured arrays. Specifically, the optimal range of array periodicity for the nanolens is $P = 450$–550 nm. In this range, the oblique angle at $\theta = 0°$–50° gives the nanolens array a larger η than the nanorod and nanocone arrays. Compared with the other nanostructures, the power conversion efficiency of the nanolens array across the periodicity of the entire array decreases more gradually with increasing oblique angle. Above discussion associated with Figures 5 and 6 suggests that the surface

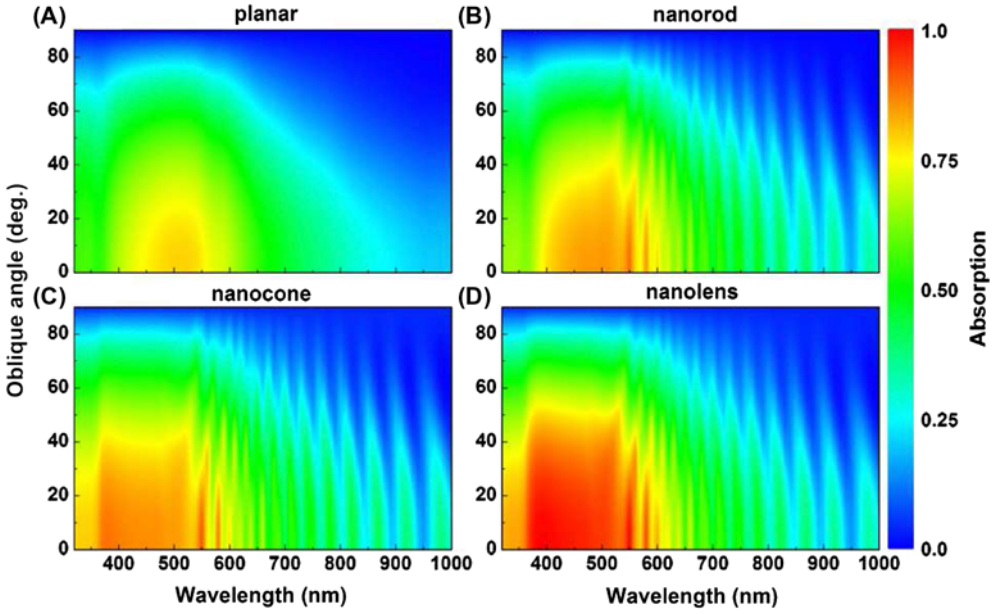

Figure 5. The optical absorption $A(\theta, \lambda)$ as a function of the incident wavelength (λ) and the oblique angle (θ) for (A) the planar thin-film and (B) the nanorod, (C) nanocone, and (D) nanolens arrays.

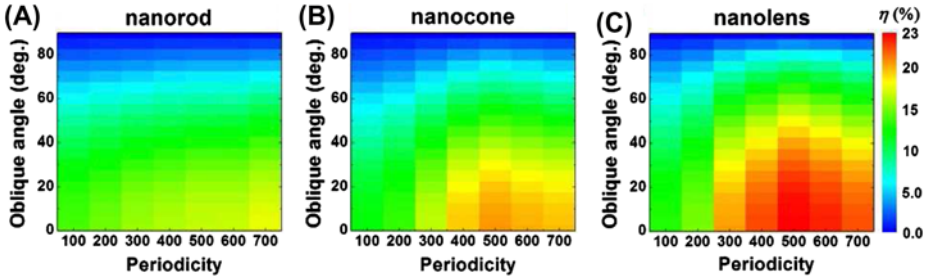

Figure 6. The power conversion efficiency vs. array periodicity and oblique angle for the (A) nanorod, (B) nanocone, and (C) nanolens arrays.

texture of the nanolens array may offer greater tolerance for fabrication imperfections and may have practical implications on the daily operation of solar cells.

4. Conclusion

In conclusion, we investigated the effect of the geometrical profile of nanostructured arrays on the performance of crystal Si thin-film solar cells. Of the three nanostructured arrays studied, the nanolens array offers excellent impedance matching between crystal Si and air through a continuous distribution of effective refractive indices along the direction of solar illumination, and it provides superior optical coupling with the incident light into in-plane guided modes. As a result, the nanolens array exhibits enhanced absorption across a wide range of wavelengths and incident angles of solar illumination. The surface texture of the nanolens array also offers greater

tolerance for fabrication imperfections and a promising way to enhance the conversion efficiency of Si thin-film solar cells.

Acknowledgments

The authors gratefully acknowledge financial support from the National Science Council of Republic of China (ROC) in Taiwan (Contract No. NSC-100-2112-M-003-006-MY3) and from the National Taiwan Normal University (award NTNU100-D-01).

References

[1] Tsakalakos L. Nanostructures for photovoltaics. Materials Science and Engineering. 2008;62 (6):175–89.
[2] Lewis NS. Toward cost-effective solar energy use. Science. 2007;315(5813):798–801.
[3] Miles RW, Zoppi G, Forbes I. Inorganic photovoltaic cells. Materials Today. 2007;10(11):20–7.
[4] Yao Y-C, Tsai M-T, Hsu H-C, She L-W, Cheng C-M, Chen Y-C, Wu C-J, Lee Y-J. Use of two-dimensional nanorod arrays with slanted ITO film to enhance optical absorption for photovoltaic applications. Optics Express. 2012;20(4):3479–89.
[5] Hägglund C, Zäch M, Petersson G, Kasemo B, Electromagnetic coupling of light into a silicon solar cell by nanodisk plasmons. Applied Physics Letter. 2008;92(5):053110-1–3.
[6] Dunbar RB, Pfadler T, Schmidt-Mende L. Highly absorbing solar cells-a survey of plasmonic nanostructures. Optics Express. 2012;20(S2):77–A189.
[7] Sun Z, Zuo X, Yang Y. Role of surface metal nanoparticles on the absorption in solar cells. Optics Letters. 2012;37(4):641–3.
[8] Diukman I, Orenstein M. How front side plasmonic nanostructures enhance solar cell efficiency. Solar Energy Materials and Solar Cells. 2011;95(9):2628–31.
[9] Hu L, Chen G. Analysis of optical absorption in Silicon nanowire arrays for photovoltaic applications. Nano Letters. 2007;7(11):3249–52.
[10] Zeng L, Bermel P, Yi Y, Alamariu BA, Broderick KA, Liu J, Hong C, Duan X, Joannopoulos J, Kimerling LC. Demonstration of enhanced absorption in thin film Si solar cells with textured photonic crystal back reflector. Applied. Physics Letter. 2008;93(22):221105-1–3.
[11] Zhang X, Gao S, He S. Optimal design of a silicon-on-insulator nanowire waveguide for broadband wavelength conversion. Progress in Electromagnetics Research. 2009;89:183–98.
[12] Li J, Yu HY, Wong SM, Li X, Zhang G, Lo PG-Q, Kwong D-L. Design guidelines of periodic Si nanowire arrays for solar cell application. Applied Physics Letter. 2009;95(24):243113-1–3.
[13] Kuang Y, van der Werf KHM, Karine HM, Houweling ZS, Schropp REI. Nanorod solar cell with an ultra thin a-Si:H absorber layer. Applied Physics Letter. 2011;98(11):113111-1–3.
[14] Lin C, Huang N, Povinelli ML. Effect of aperiodicity on the broadband reflection of silicon nanorod structures for photovoltaics. Optics Express. 2012;20(S1):A125–32.
[15] Zhu J, Yu ZF, Burkhard GF, Hsu CM, Connor ST, Xu YQ, Wang Q, McGehee M, Fan SH, Cui Y. Optical absorption enhancement in amorphous silicon nanowire and nanocone arrays. Nano Letters. 2009;9(1):279–82.
[16] Lu Y, Lal A. High-efficiency order silicon nano-conical-frustum array solar cell by self-powered parallel electron lithography. Nano Letters. 2010;10(11):4651–6.
[17] Lee SH, Zhang X-G, Parish CM, Lee HN, Smith DB, He Y, Xu J. Nanocone tip-film solar cells with efficient charge transport. Advanced Materials. 2011;23(38):4381–5.
[18] Li K, Stockman MI, Bergman DJ. Self-similar chain of metal nanospheres as an efficient nanolens. Physical Review Letters. 2003;91(22):227402-1–4.
[19] Čampa A, Krč J, Topič M. Analysis and optimisation of microcrystalline silicon solar cells with periodic sinusoidal textured interfaces by two-dimensional optical simulations. Journal of Applied Physics. 2009;105(8):083107-1–5.
[20] Zhu J, Hsu C-M, Yu Z, Fan S, Cui Y. Nanodome solar cells with efficient light management and self-cleaning. Nano Letters. 2010;10(6):1979–84.
[21] Kim B, Bang J, Jang S, Kim D, Kim J. Surface texturing of GaAs using a nanosphere lithography technique for solar cell applications. Thin Solid Films. 2010;518(22):6583–6.
[22] Bozzola A, Liscidini M, Andreani LC. Photonic light-trapping versus Lambertian limits in thin film silicon solar cells with 1D and 2D periodic patterns. Optics Express. 2012;20(S2):A224–44.

[23] Berginc G, Bourrely C, Ordenovic C, Torr'esani B. A numerical study of absorption by multilayered biperiodic structures. Progress In Electromagnetics Research. 1998;19:199–222.
[24] Hernandez-Lopez MA, Quintillan M. Propagation characteristics of modes in some rectangular waveguides using the finite-difference time-domain method. Journal of Electromagnetic Waves and Applications. 2000;14(12):1707–22.
[25] Aspnes DE. Optical properties of thin films. Thin Solid Films. 1982;89(3):249–62.
[26] Bermel P, Luo C, Zeng L, Kimerling LC, Joannopoulos JD. Improving thin-film crystalline silicon solar cell efficiencies with photonic crystals. Optics Express. 2007;15(20):16986–1700.
[27] Smestad GP. Optoelectronics of solar cells. Washington (DC): SPIE Press; 2002.
[28] ASTMG173–03. Standard tables for reference solar spectral irradiances: direct normal and hemispherical on 37 degree tilted surface. West Conshohocken, PA: ASTM International; 2005.
[29] Chen F, Shen Q, Zhang L. Electromagnetic optimal design and preparation of broadband ceramic radome material with graded porous structure. Progress In Electromagnetics Research. 2010;105:445–61.
[30] Liu Y, Sun SH, Xu J, Zhao L, Sun HC, Li J, Mu WW, Xu L, Chen KJ. Broadband antireflection and absorption enhancement by forming nano-patterned Si structures for solar cells. Optics Express. 2011;19(S5): A1051–6.
[31] Zhou L, Pei Y, Zhang R, Fang D. Optimal design for high-temperature broadband radome wall with symmetrical graded porous structure. Progress In Electromagnetics Research. 2012;127:1–14.
[32] Palik ED. Handbook of optical constants of solids. New York (NY): Academic Press; 1998.
[33] Zhu B, Wang Z, Huang C, Feng Y, Zhao J, Jiang T. Polarization insensitive metamaterial absorber with wide incident angle. Progress In Electromagnetics Research. 2010;101:231–9.
[34] He XJ, Wang Y, Wang J, Gui T, Wu Q. Dual-band terahertz metamaterial absorber with polarization insensitivity and wide incident angle. Progress In Electromagnetics Research. 2011;115:381–97.
[35] Huang L, Chen H. Multi-band and polarization insensitive metamaterial absorber. Progress In Electromagnetics Research. 2011;113:103–10.